Experimental Investigation of Dynamics Effects on Multiple-Injection Common Rail System Performance

Andrea E. Catania
Alessandro Ferrari
Michele Manno
Ezio Spessa

IC Engines Advanced Laboratory,
Dipartimento di Energetica,
Politecnico di Torino,
C.so Duca degli Abruzzi, 24
10129–Torino, Italy

Fundamental aspects of Common Rail (CR) fuel-injection-system dynamics were investigated, paying specific attention to the wave propagation induced pressure oscillations and to their relationships with the system control parameters and multiple-injection performance. A detailed experimental analysis of the pressure-wave propagation phenomena in a last-generation CR Multijet equipment of the solenoid type was carried out on a high performance new test-bench Moehwald-Bosch MEP2000-CA4000 under real engine simulated conditions. The experimental results include pressure time histories in the rail and at the injector inlet, as well as flow-rate patterns, for both single and multiple injection events. The measured volume of fuel injected at each injection pulse is also reported. The analysis of the system oscillating behavior was carried out with the support of a simple lumped parameter model. Such a model was shown to be capable of predicting the main frequencies of the hydraulic circuit and their dependence on the geometrical parameters. The good agreement between the outcome of this simple model and the experimental data also substantiated the reliable authors' interpretation of the primary cause and effect relations underlying the complex flow phenomena occurring in the system. A refined computational model was developed and validated in a parallel work, providing a hydrodynamic analysis tool that is complementary to experimentation and also a means of hydraulic-system layout design and optimization. Finally, the mutual fluid-dynamic interactions taking place between consecutive injection events by distinct injectors of the same system are investigated in addition to the difference in dynamics of valve covered orifice and Minisac-nozzle injectors. Cycle-to-cycle variations in system performance were also investigated. [DOI: 10.1115/1.2835353]

Introduction

The Common Rail (CR) diesel injection system, which was cast in production approximately ten years ago [1,2], has met an extraordinary success and is responsible of the ever-increasing share of diesel engines in the European automotive market. The main key to this success is the flexibility that can be provided for the most important injection parameters: The pressure level generation is almost independent of the engine speed and of fuel metering; the injection timing and duration can be optimized for every working condition.

The emission regulations have imposed further refinements on CR systems, in order to achieve both optimal fuel consumption and exhaust emissions. The ability of delivering multiple injections, which is one of the most interesting features of such injection systems, allows an improved combustion and heat-release-rate control, resulting in clean and efficient engine performance, especially in conjunction with variable swirl and cooled exhaust gas recirculation (EGR). To achieve this result, CR electroinjectors have thoroughly been investigated by researchers of the automotive field, in order to obtain fast actuations, retaining, at the same time, a good precision of the injected fuel volume.

However, the dynamics of CR hydraulic components can cause sensible perturbations to multiple injections, which hence occur under different conditions from those expected. The wave propagation phenomena arising in the system, subsequent to an injection event, lead to pressure oscillations that influence the injected fuel quantity, particularly when the dwell time between consecutive injections is changed [3]. The dependence of the injected quantity on the system dynamics was also pointed out by other authors [4–7]. The rail pressure is also affected by the system dynamics: Whenever an injection occurs, the pressure in the rail drops because the rail itself does not behave as an infinite volume capacity [3,6]. A sensor for continuously monitoring the pressure at the injector inlet was proposed in Ref. [8] to deliver information to the engine electronic control unit (ECU) and thus adjust the injection parameters, so as to better control the injected fuel quantity. Nevertheless, no one of the above-mentioned works reports a detailed analysis of the pressure-wave propagation phenomena and an investigation of their relationship with the ECU control parameters, system hydraulic layout, and performance.

The present work aims at further investigating the complex dynamic phenomena, which take place in a CR fuel-injection system, with specific attention to the multiple-injection performance, following the work started in Ref. [3], so as to give a contribution to the knowledge of the cause and effect relations underlying the system operation.

The presented experimental results include time histories of the pressure in the rail and at the injector inlet, as well as of flow rate, for both single and multiple injections. The measured volume of fuel injected on each injection pulse is also reported. The influence of the system dynamics on its performance was analyzed. A simple lumped parameter model was developed and applied to better understand the system oscillating behavior. More specifically, it was shown how such a model is capable of predicting the main frequencies of the hydraulic circuit and their dependence on the geometrical parameters. The good agreement between the results of this simple model and the experimental data also sup-

Manuscript received April 13, 2007; final manuscript received November 9, 2007; published online March 28, 2008. Review conducted by Margaret Wooldridge. Paper presented at the ICES 2005.

Fig. 1 Test bench

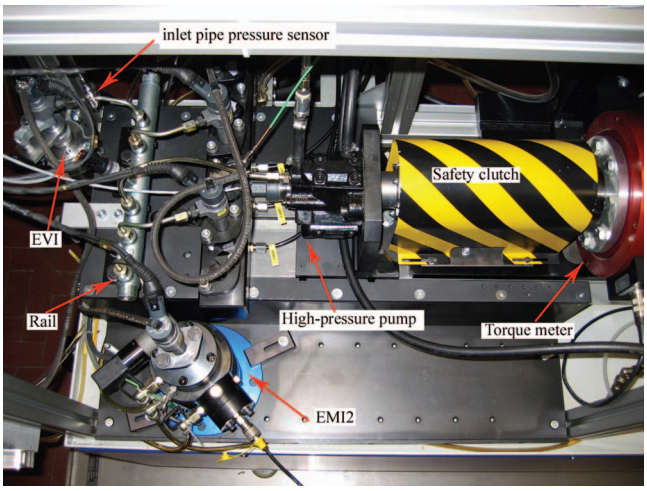

Fig. 3 CR injection-system layout and measuring instruments

ported the reliable authors' interpretation of the cause and effect main relationships governing the complex flow phenomena that occur in the system. A refined computational model was developed and validated in Ref. [9] to provide a hydrodynamic analysis tool complementary to experimentation and a means of hydraulic-system layout design and optimization.

Finally, the mutual fluid-dynamic interactions taking place between consecutive injection events by distinct injectors of the same system were investigated, in addition to the difference in dynamics of valve covered orifice (VCO)- and Minisac-nozzle injectors. Cycle-to-cycle dispersion of system performance was also analyzed.

Experimental Facility

The experiments were carried out on a high performance test-bench Moehwald-Bosch MEP2000-CA4000, recently set up at the IC Engines Advanced Laboratory (ICEAL) of Politecnico di Torino (Figs. 1–3). This facility, having maximum shaft speed and power of 6100 rpm and 35 kW, respectively, is capable of simulating real engine working conditions and also injection-system transient operations. It is equipped with several devices to precisely control shaft speed, oil temperatures, pump feeding pressure, and backpressure at the injectors' pilot valve discharge.

The experimental apparatus includes the following main measuring instruments: The volumetric device EMI2 gauging the injected volume and capable of separately measuring the volume discharged at each shot in multiple injections, the injection-rate indicator EVI of the Bosch type [10], piezoresistive sensors for monitoring the pressures in the rail and at the injector inlet (11 and 12 in Fig. 2), and fluid-temperature sensors. A high precision shaft-torque meter and a needle-lift sensor were also installed.

A National Instruments data acquisition system, provided with homemade acquisition software in LABVIEW programming environment, was used to monitor the system.

Injection System. A second-generation CR injection system of the Multijet solenoid type was considered, made up of a Radialjet CP1 high-pressure pump, 0.550 cm^3/rev in displacement, and of four electroinjectors with either Minisac or VCO nozzles. A 20 cm^3 rail volume and inlet pipes of length 125 mm and diameter 2.4 mm were used. The ISO-4113 oil was used as working fluid, suitable to simulate the diesel fuel. Figures 2 and 3 show the injection-system layout on the test bench and the location of main measuring instruments. Previous tests were made to select the four

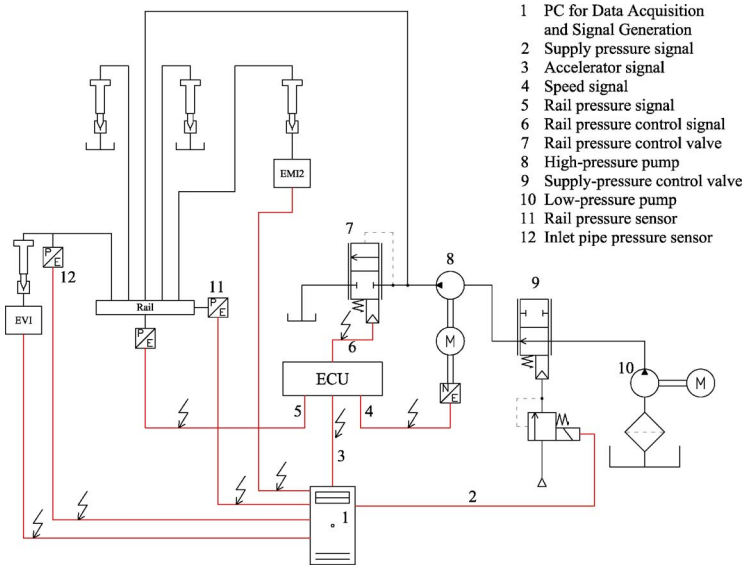

Fig. 2 Test-bench layout and instrumentation

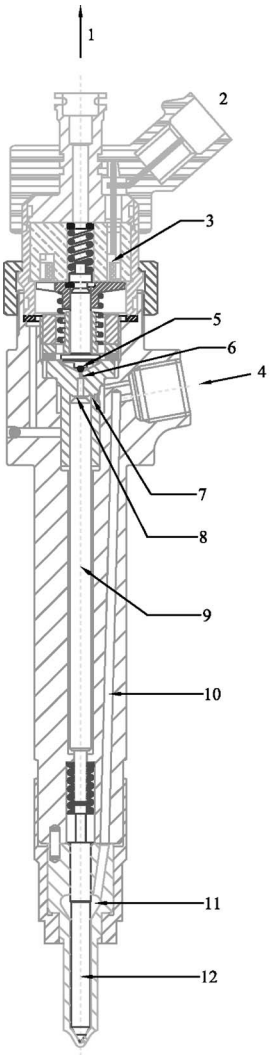

1 Fuel return (low pressure)
2 Electrical connection
3 Triggering element (solenoid valve)
4 Fuel inlet from the rail (high pressure)
5 Valve ball
6 Bleed orifice
7 Feed orifice
8 Valve control chamber
9 Valve control plunger
10 Feed pipe to the nozzle
11 Delivery chamber
12 Nozzle needle

Fig. 4 Electroinjector

injectors with negligible nozzle-to-nozzle variations. Figure 4 gives a detailed electroinjector drawing. An extensive description of the CR system working principles is reported in Ref. [11].

EMI2 Injected Volume Meter. The EMI2 gauges the displacement of a piston that runs in the injection chamber (Fig. 5) by means of a linear variable differential transformer (LVDT). The injected volume is thus determined. A temperature sensor allows

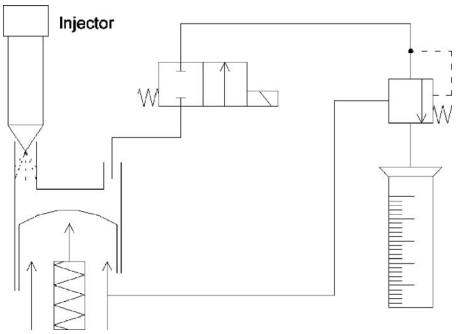

Fig. 5 EMI2 operation scheme

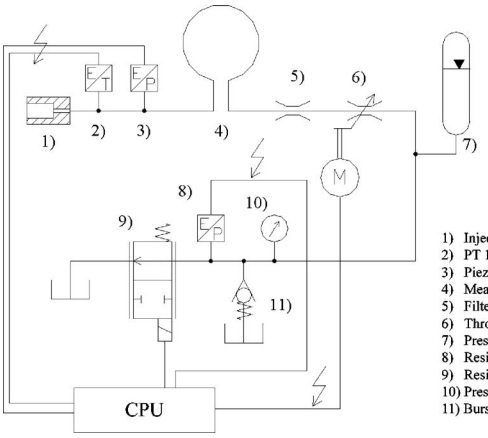

1) Injector-tip adapter
2) PT 100 Temperature sensor
3) Piezoelectric pressure sensor
4) Measuring tube loop
5) Filter package
6) Throttle valve
7) Pressure accumulator
8) Residual-pressure sensor
9) Residual-pressure control valve
10) Pressure gauge
11) Bursting disk

Fig. 6 EVI operation scheme

to evaluate the fluid density and thus to calculate the injected mass. The maximum injected volume is 600 mm^3, with a relative precision of $\pm 0.1\%$.

EVI Injection Discharge-Rate Indicator. The injection takes place into an oil-filled measuring tube (4 in Fig. 6). The fuel discharge gives rise to a pressure wave, whose amplitude is related to the actual discharged flow rate, as will be shown. Oil temperature and pressure were gauged at the initial part of the measuring tube loop (2 and 3 in Fig. 6), downstream from the injector tip adapter (i.e., 1 in Fig. 6). The EVI electronic control unit is able to precisely control the residual pressure in the system (8 and 9 in Fig. 6), so that accurate and repeatable measurements could be carried out.

The actual injected mass flow rate can be evaluated, on the basis of the pressure signal monitored by Sensor 3, as follows. The injection-induced pressure wave travels downstream with a speed $a+u$ [12]. The fluid behind the perturbations has a velocity $u+du$ and a pressure $p+dp$, while the fluid in front of the wave has velocity and pressure u and p (Fig. 7). Considering a moving frame of reference, integral with the compression wave (Fig. 8), the fluid velocity is $a-du$ behind the wave, and a in front of this, so that the mass conservation equations, for an infinitesimal control volume containing the wave front, can be written as follows:

$$\rho a A = (a - du)(\rho + d\rho)A \tag{1}$$

where A represents the pipe cross section. The density rise is

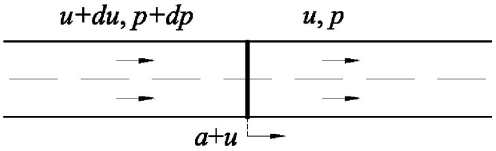

Fig. 7 Pressure wave in the EVI measuring tube

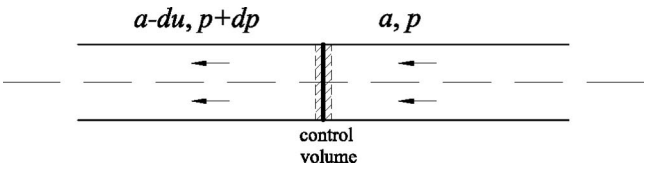

Fig. 8 Reference frame integral with the compression wave in the EVI measuring tube

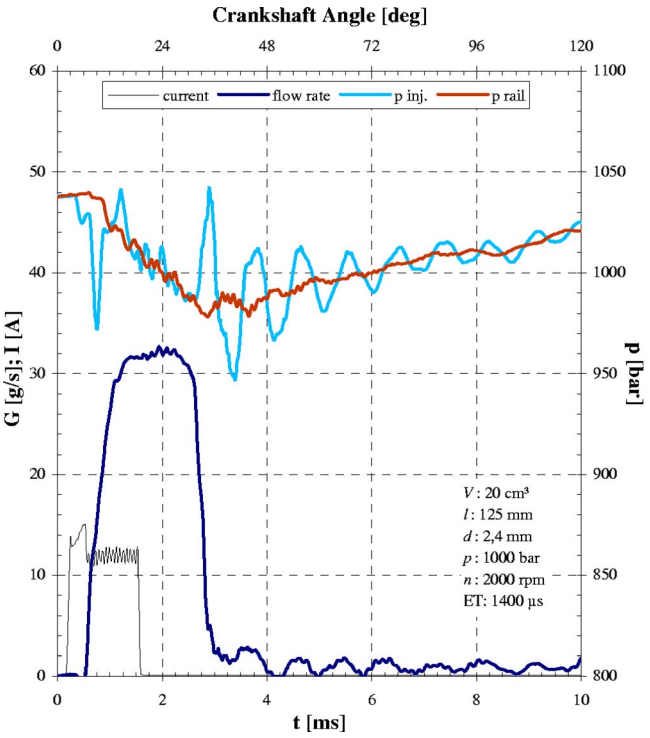

Fig. 9 Pressure, flow rate, and current time histories for ET =1400 μs

$$d\rho = \rho \frac{du}{a} \tag{2}$$

The momentum balance for the control volume yields

$$(\rho + d\rho)(a - du)^2 A - \rho a^2 A = -A dp \tag{3}$$

and thus the pressure rise results:

$$dp = 2\rho a du - a^2 d\rho \tag{4}$$

Combining Eqs. (2) and (4), it is possible to evaluate the velocity change due to the pressure wave:

$$du = \frac{dp}{\rho a} \tag{5}$$

The volume and mass flow rates are then easily calculated by a numerical integration:

$$Q(t) = A \int_0^t du \qquad G(t) = A \int_0^t \rho du \tag{6}$$

Results and Discussion

Single Injection. The system performance was investigated first by a careful analysis of dynamic phenomena occurring for a single injection. Figure 9, which refers to an energizing time (ET) of 1400 μs and to a rail-pressure level of 1000 bars, shows the system behavior during and after the injection event, in terms of rail pressure, injector inlet pressure, injected mass flow rate, and electrical current. The flow-rate fluctuations that appear after the injection event are due to wave reflections at the piezotransducer seat and at the injector tip adapter.

The rail-pressure drop, due to the injector opening, and the pipe-pressure rise induced by its closure are easily recognizable in the figure, which also makes clear that the rail pressure is not constant, as is taken in Ref. [4] instead, but undergoes a reduction of about 50 bars under these conditions. Moreover, examining the current and flow-rate patterns, one can infer that the injection is

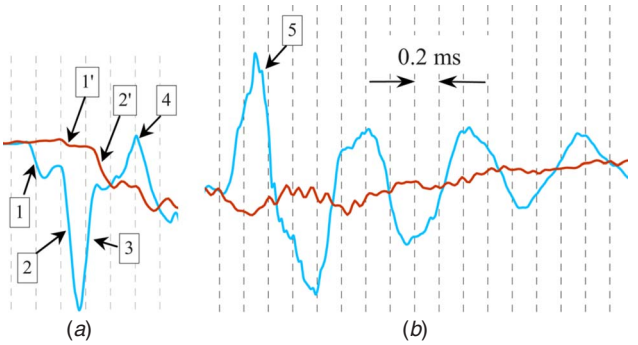

Fig. 10 Pressure waves (*a*) at the start and (*b*) at the end of injection

delayed and is longer than the current signal, whose duration on the contrary is almost coincident with the pilot valve opening time, due to the fast dynamic response of this valve [9].

By a thorough examination of the pressure time histories in Fig. 10, which amplifies pressure signal portions of Fig. 9, it is possible to recognize several interesting phenomena that occur within the injection system soon after the ECU has started the current signal to the electroinjector. The dashed vertical lines visible in this figure are set at intervals of 0.2 ms.

The pressure drop at the injector inlet, marked with 1 in Fig. 10, can be ascribed to the rarefaction wave set off by the sudden opening of the pilot valve. In fact, it is clear from this figure that such pressure drop takes place immediately after the current flows through the solenoid. The rarefaction wave has also effect on the rail pressure, which undergoes a slight drop, marked with 1′ in the figure, occurring about 0.2 ms later than that at the injector inlet. Such a delay is due to the finite propagation speed of the rarefaction wave.

After the opening of the pilot valve, the pressure in the valve control chamber (Fig. 4) rapidly decreases, and thus the nozzle needle starts moving upward, causing a flow rate to be discharged from the injector (Fig. 9). These events trigger another rarefaction wave, which starts at the needle seat and travels upward. Its effects are visible in Fig. 10(*a*) as pressure drops marked with 2 (on the inlet pressure signal) and with 2′ (on the rail-pressure trace).

When this rarefaction wave arrives at the rail, it is reflected as a compression wave, which aims at restoring the original pipe pressure. Such a compression wave reaches the injector inlet and determines a pressure rise, marked as 4 in Fig. 10(*a*). In fact, it is evident that the time delay between 2 and 2′ is the same as between 2′ and 4.

Therefore, the pressure rise marked as 3 must have nothing to do with the rail. In fact, as soon as the needle lift approaches its maximum value, there is no more rarefaction generated, but on the contrary the nozzle orifices determine a flow restriction and thus cause a compression wave to start from the nozzle and move upward. Hence, the pressure rise marked with 3 has to be associated to this latter compression wave [9]. This statement will also be confirmed in the following section, where the effects of two different nozzles (Minisac and VCO) will be compared.

At the end of injection, the needle closure creates a water-hammer effect, so that yet another compression wave arises at the nozzle and travels upward. This event is visible in Fig. 10(*b*) as the pressure peak marked with 5. From now on, the system is completely closed (both the pilot valve and the needle valve are closed) and therefore this compression wave, being reflected in turn by the rail and by the needle, produces the oscillating behavior evident in Figs. 10(*b*) and 9.

It should be pointed out that the presence of all the events shown in Fig. 10(*a*) does not depend on the injection duration (and thus on ET), because these take place whenever the pilot and the needle valves open. On the other hand, the water-hammer

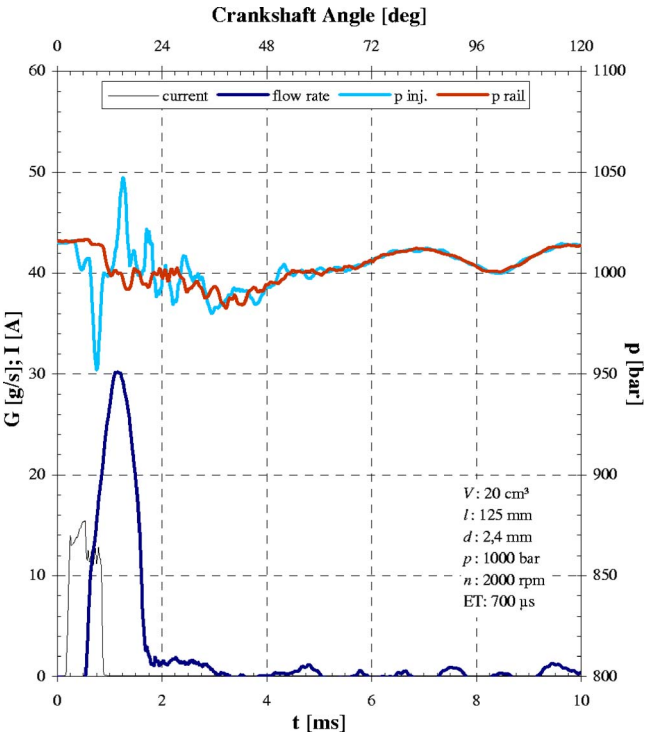

Fig. 11 System response for ET=700 μs

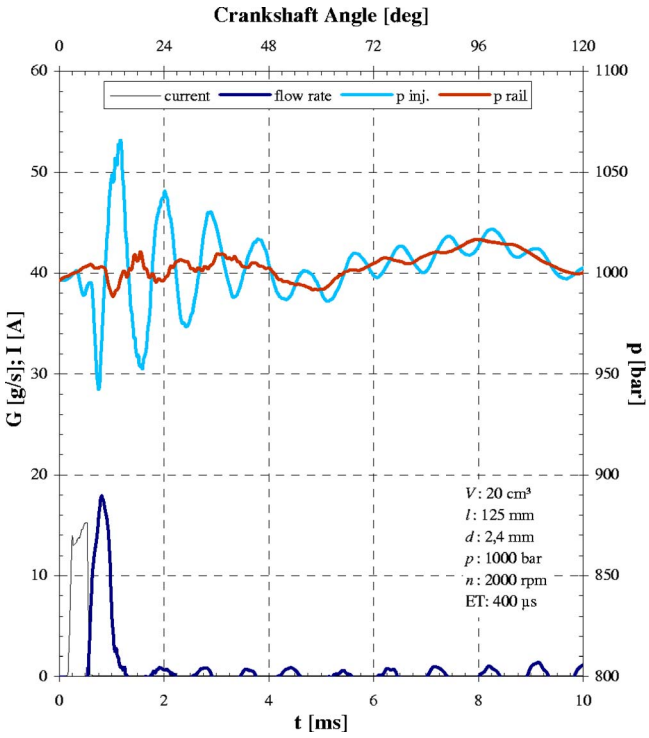

Fig. 12 System response for ET=400 μs

event (5) evidenced in Fig. 10(*b*) is obviously dependent on ET, because it takes place when the needle closes. Therefore, for smaller ET, the time interval between the two pressure peaks marked with 4 and 5 in Fig. 10 becomes smaller as well. As a consequence, both Peak 5 and the resulting oscillations have an amplitude that depends on the ET due to the pressure-wave interactions (which can take place with amplifying or damping effects). The amplitude generally grows with ET (Figs. 9 and 11). Obviously, the hydraulic shear resistances that are present in the system progressively damp the induced oscillations, so that these can disappear before the next injection cycle (Fig. 11).

Figures 11 and 12 show the system response to ETs of 700 and 400 μs, respectively, to highlight how markedly the oscillation amplitude can be influenced by the injection duration. In particular, for small injected quantities (Fig. 12), typical of pilot injections, the oscillations can be remarkable when a resonance occurs, with the merging of Peaks 4 and 5 (Fig. 10). These will affect the subsequent injection, in the case of multiple injections.

Multiple Injections. When, for example, a pilot and a main injection are performed, the pressure oscillations triggered by the pilot injection can have a sensible influence on the subsequent main injection. Figure 13 illustrates the injected volumes for pilot and main injections as functions of the dwell time (DT), that is, the time interval between the end of the pilot-injection current signal and the start of the main-injection current signal:

$$\mathrm{DT} = \left| \frac{\mathrm{SOI}_{\mathrm{main}} - \mathrm{SOI}_{\mathrm{pil}}}{\omega} \right| - \mathrm{ET}_{\mathrm{pil}} \tag{7}$$

This temporal interval is directly related, through the engine speed and the pilot ET, to the starts of the pilot and main injections (i.e., to the instants when the current pulses to the solenoid start), which are expressed as crank angles before top dead center. The test results shown in Fig. 13 were obtained keeping $\mathrm{SOI}_{\mathrm{main}}$ constant at 0 deg and getting the pilot and main injections gradually closer by increasing $|\mathrm{SOI}_{\mathrm{pil}}|$.

It is evident from Fig. 13 that V_{pil} keeps fairly constant with DT, whereas V_{main} shows sensible oscillations as DT varies. Such phenomenon is explained by the pressure oscillations described in the previous paragraph. In particular, it is not surprising that if the main injection takes place when the "opening pressure" (that is, the injection pressure when the needle starts opening) reaches a maximum, the corresponding injected volume will be maximum, and vice versa. The inlet pressure and the injection pressure are closely related, as can be inferred by experimental results, by way of identifying the opening pressure on the inlet pressure time history, taking in mind that there is a slight delay mainly due to the length of the injector drilled passage [9].

In fact, Fig. 14 illustrates the flow processes occurring in the injection system for a DT of 1825 μs, which corresponds to a maximum injected volume (Fig. 13). The arrow in the picture indicates a maximum of pressure at the injector inlet, virtually corresponding to a maximum of pressure in the injector delivery chamber, when the needle valve starts opening. Such a pressure indicates what is intended as nozzle opening pressure, which in this case is very close to a maximum.

On the other hand, Fig. 15 illustrates the system response when the DT is 2300 μs, i.e., a value corresponding to a minimum main injected volume (Fig. 13). In this case, the main injection starts when the opening pressure is around a minimum, as is pointed out by the arrow in Fig. 15.

It is interesting to more closely analyze the relation between the opening pressure and the injected volume. One spontaneous preliminary hypothesis to establish such a relation might be that higher opening pressures imply higher injection pressures along the whole injection event, which would obviously result in higher injected volumes. However, Figs. 14–16, together with other test results, point out that the difference between pressure time histories during the main injection, resulting from the value of the opening pressure, is not much significant, mean pressure being almost the same during injection, and hence such a difference must not be taken as responsible for the different injected volumes. Additional considerations can be drawn from Fig. 16, which compare the mass flow rates for the two main injections shown in Figs. 14 and 15. The nozzle opening delay with respect to the current signal is clearly dependent on the opening pressure: The

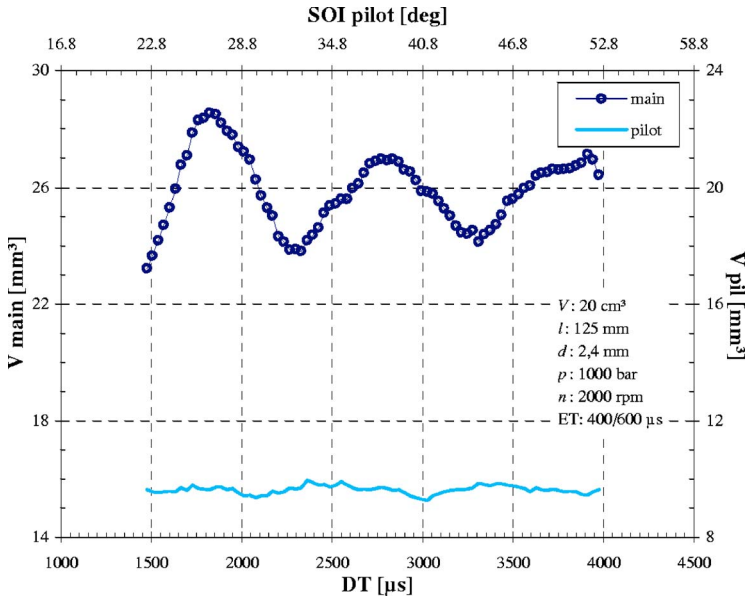

Fig. 13 Injected volumes for pilot and main injections at p_{rail}=1000 bars

higher this pressure is, the lower the delay is. In fact, it results that for DT of 1825 μs (maximum opening pressure), the delay is approximately 350 μs, whereas for DT of 2300 μs (minimum opening pressure), the delay is approximately 380 μs. Such a difference can be explained by considering that if the opening pressure is higher, the force resulting from the pressure actions on the needle valve and control plunger at the nozzle delivery chamber, and within the valve control chamber reaches more quickly the value that determines the nozzle opening. However, this is not the only difference notable in Fig. 16; it is also evident that for the higher opening pressure, the nozzle closes later. A reason for this must be sought in the control chamber dynamics, possibly by means of an accurate numerical model [9], as done in Ref. [13], because experimental data on such a dynamics are very difficult, if not almost impossible, to be acquired.

Therefore, the combined effects of a shorter nozzle opening delay and a retarded nozzle closure result in an injection duration that is much longer in the case of the higher opening pressure, so that the true reason for the different injected volumes has to be found in injection durations rather than in injection pressures. Actually, Fig. 16 also shows that the flow rate can reach higher maximum values for lower opening pressures. This is true when

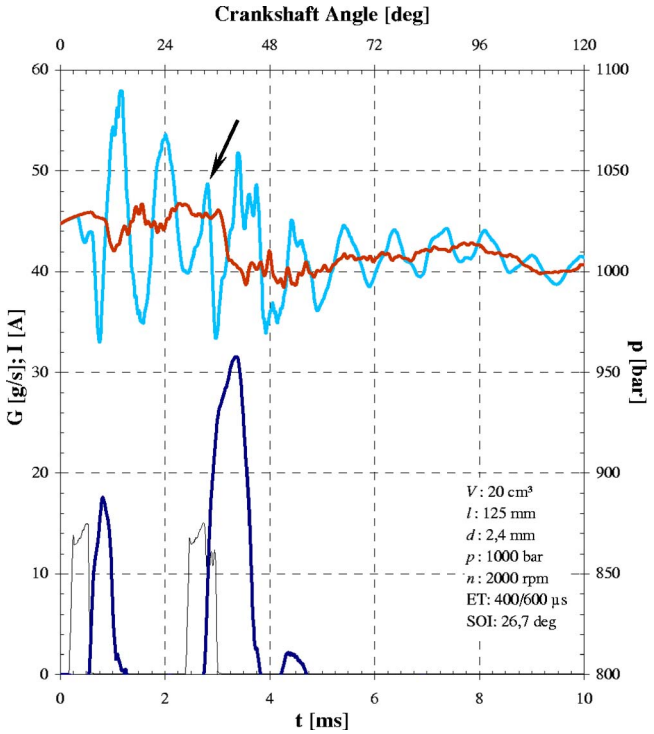

Fig. 14 System response at p_{rail}=1000 bars, ET=400/600 μs, and DT=1825 μs

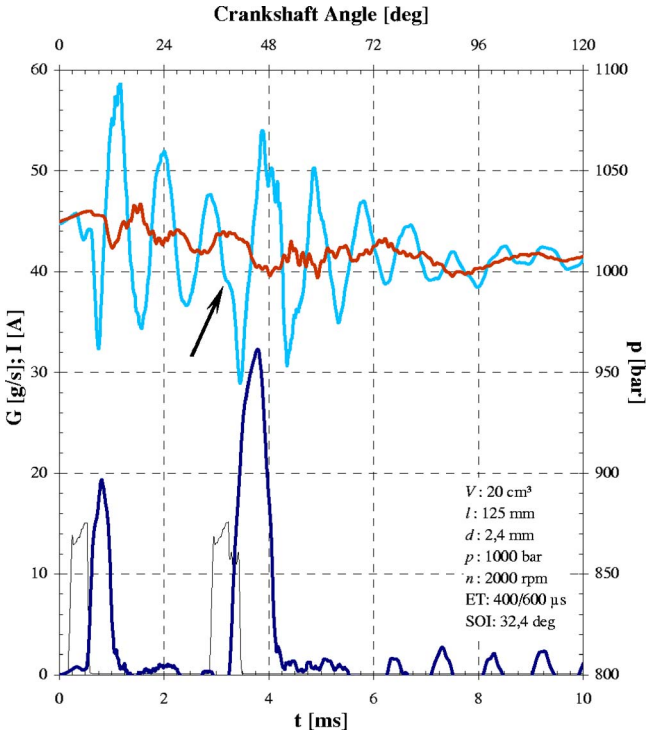

Fig. 15 System response at p_{rail}=1000 bars, ET=400/600 μs, and DT=2300 μs

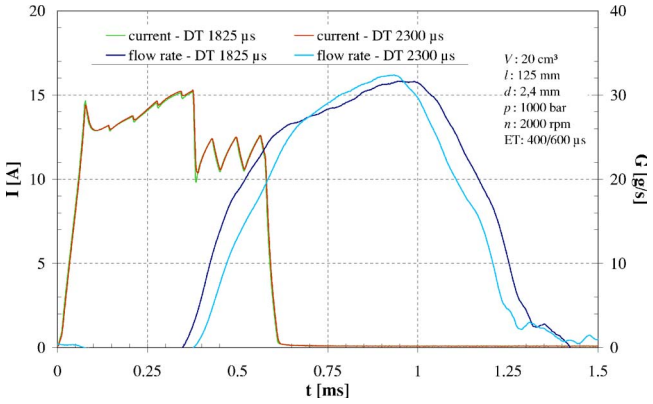

Fig. 16 Comparison between injected flow rates for different DT and same ET

the ET is not too small, i.e., longer than 500 μs, as is usually the case for main injections. Otherwise, if ET is shorter than such a value, then also the maximum injected flow rate depends on the opening injection pressure; however, this is a more common case for pilot or postinjections.

In summary, the main variable affecting the injected volume is the nozzle opening pressure, which exerts its influence through the injection duration. This also explains why the inlet pressure oscillations after injections in Figs. 14 and 15 and the injected volume oscillations in Fig. 13 share the same frequency, i.e., nearly 0.85 ms for the hydraulic-system layout under investigation.

All the above remarks hold for various injection conditions. For example, with p_{rail}=1250 bars and ET of 400 and 900 μs for pilot and main injections, respectively, the injected volume varies as a function of DT according to Fig. 17. Besides, with the same p_{rail}=1250 bars, Fig. 18 shows the system behavior for DT =1755 μs, corresponding to a maximum main injected volume, whereas Fig. 19 presents the results for DT=2230 μs, which corresponds to a minimum main injected volume.

Once again, from a careful examination of the injected flow-rate time history, it can be deduced that high opening pressures give rise to high injected volumes through an increase of the injection duration by both advancing the nozzle opening and delaying its closure (Fig. 20).

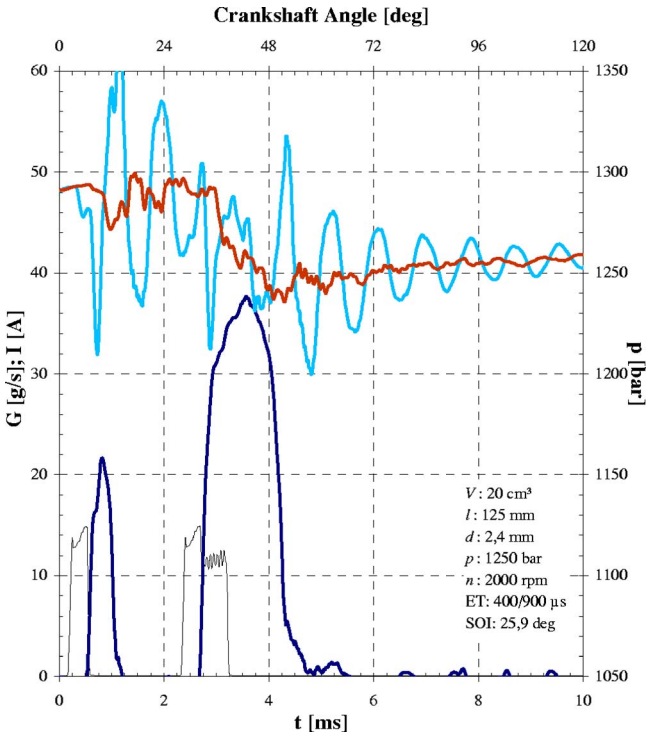

Fig. 18 System response at p_{rail}=1250 bars, ET=400/900 μs, and DT=1755 μs

Moreover, observing the differences between the flow-rate patterns in Fig. 20, it is evident that the injection pressure, which directly shapes the injected flow rate, has an oscillating behavior conforming to that of the inlet pressure.

Lumped Parameter Model. The aforementioned oscillating behavior can be interpreted by a lumped parameter model of the subsystem including rail, inlet pipe, and injector. These components can be thought of as being made up of hydraulic capacitances and inductances. The hydraulic resistances that can be as-

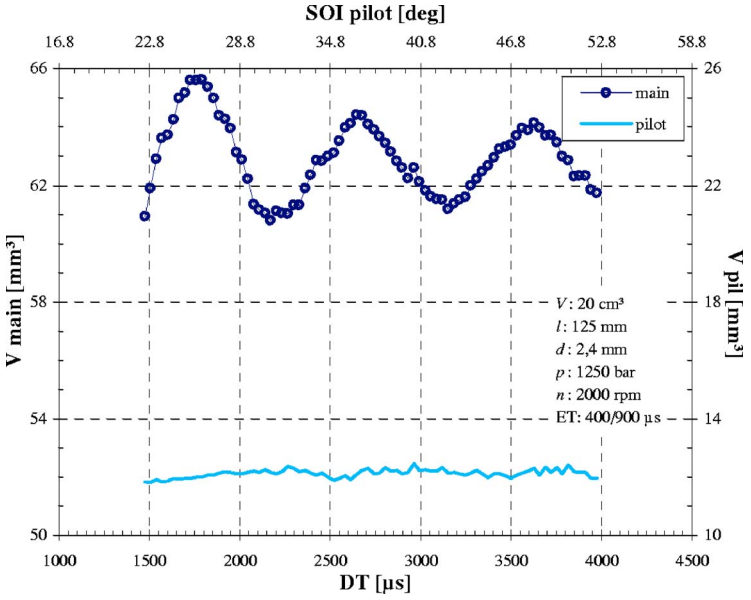

Fig. 17 Injected volumes of pilot and main injections at p_{rail}=1250 bars

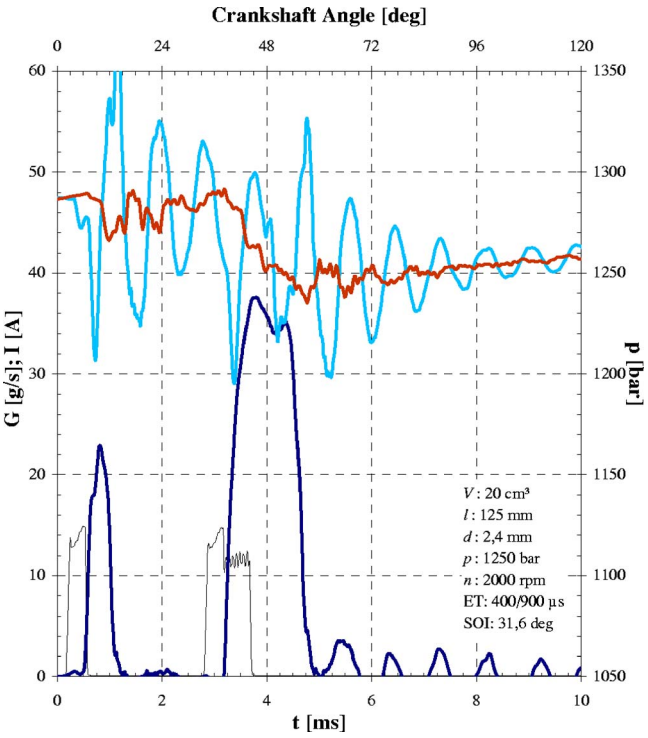

Fig. 19 System response at p_{rail}=1250 bars, ET=400/900 μs, and DT=2230 μs

sociated to the distributed viscous friction losses were neglected because the model has the main purpose of analyzing the system circular frequencies and these are scarcely influenced by the hydraulic resistances.

The system can be schematically described as in Fig. 21, where the rail is connected to the injector through the inlet pipe, which ends at a volume including the valve control chamber and filter volume effects. The feed pipe (marked with 10 in Fig. 4) starts from this volume and terminates at the delivery chamber (11 in Fig. 4). The model does not take any injected mass flow rate into account, because its purpose is to characterize the free oscillations taking place after the needle closure.

The symbols used in Fig. 21 have the following meanings. C_0 is the rail hydraulic capacitance, C_1 is the hydraulic capacitance of the inlet-pipe and upstream-injector volumes, C_2 is the feed pipe and delivery-chamber hydraulic capacitance, G_{01} is the mass flow rate through the inlet pipe, G_{12} is the mass flow rate through the

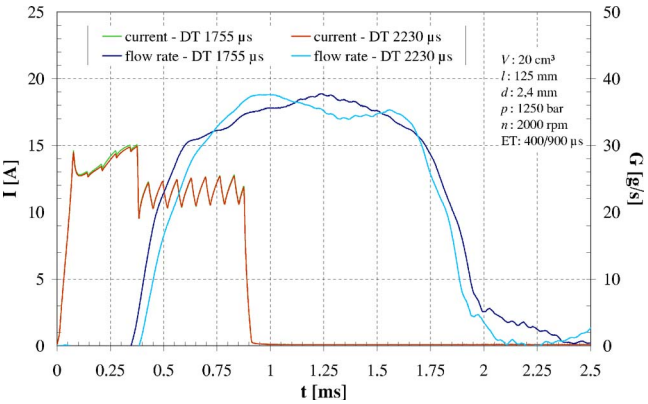

Fig. 20 Comparison between main injected flow rates at p_{rail} =1250 bars

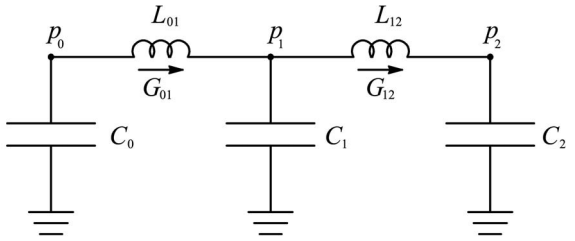

Fig. 21 Rail-pipe-injector *LC* model

feed pipe, L_{01} is the inlet-pipe hydraulic inductance, L_{12} is the feed-pipe hydraulic inductance, p_0 is the rail pressure, p_1 is the pressure upstream of the feed pipe, and p_2 is the delivery-chamber pressure.

The hydraulic capacitance and inductance are defined as

$$C = \frac{V}{a^2} \tag{8}$$

$$L = \frac{l}{A} \tag{9}$$

It should be pointed out that the volumes V, which give rise to hydraulic capacitances, could include both chambers, i.e., zero-dimensional elements, and pipes, that is, one-dimensional elements, which are thus reduced to zero-dimensional elements by spatial integration.

The model equations for the capacitance discharge are

$$\frac{dp_0}{dt} = -\frac{G_{01}}{C_0} \quad \frac{dp_1}{dt} = \frac{G_{01} - G_{12}}{C_1} \quad \frac{dp_2}{dt} = \frac{G_{12}}{C_2} \tag{10}$$

and the inductance equations write

$$L_{01}\frac{dG_{01}}{dt} = p_0 - p_1 \quad L_{12}\frac{dG_{12}}{dt} = p_1 - p_2 \tag{11}$$

By taking the time derivative of Eq. (11), and combining with Eq. (10), one obtains the following two-degree of freedom equation system, whose unknowns are the mass flow rates:

$$L_{01}\frac{d^2G_{01}}{dt} + \left(\frac{1}{C_0} + \frac{1}{C_1}\right)G_{01} - \frac{1}{C_1}G_{12} = 0$$

$$L_{12}\frac{d^2G_{12}}{dt} - \frac{1}{C_1}G_{01} + \left(\frac{1}{C_1} + \frac{1}{C_2}\right)G_{12} = 0 \tag{12}$$

This equation system can be put in matrix form as follows:

$$\mathbf{L}\ddot{\mathbf{G}} + \mathbf{K}\mathbf{G} = \mathbf{0} \tag{13}$$

where

$$\mathbf{L} = \begin{bmatrix} L_{01} & 0 \\ 0 & L_{12} \end{bmatrix} \tag{14}$$

$$\mathbf{K} = \begin{bmatrix} (1/C_0) + (1/C_1) & -1/C_1 \\ -1/C_1 & (1/C_1) + (1/C_2) \end{bmatrix} \tag{15}$$

$$\mathbf{G} = \begin{bmatrix} G_{01} \\ G_{12} \end{bmatrix} \tag{16}$$

The circular frequencies are given by the eigenvalues of the matrix $\mathbf{L}^{-1}\mathbf{K}$:

$$\mathbf{L}^{-1}\mathbf{K} = \begin{bmatrix} 1/L_{01}((1/C_0) + (1/C_1)) & -1/C_1L_{01} \\ -1/C_1L_{12} & 1/L_{12}((1/C_1) + (1/C_2)) \end{bmatrix} \tag{17}$$

which can also be written as

$$\mathbf{L}^{-1}\mathbf{K} = \begin{bmatrix} \omega_{01}^2 & -1/C_1L_{01} \\ -1/C_1L_{12} & \omega_{12}^2 \end{bmatrix} \tag{18}$$

where ω_{01} is the circular frequency associated to the system that includes rail, inlet pipe, and injector upstream volumes, and ω_{12} is the circular frequency of the system containing injector upstream volumes, feed pipe, and delivery chamber.

The resulting circular frequencies for the whole system are

$$\omega^2 = \frac{\omega_{01}^2 + \omega_{12}^2}{2} \mp \sqrt{\left(\frac{\omega_{01}^2 + \omega_{12}^2}{2}\right)^2 - \frac{1}{L_{01}L_{12}}\left(\frac{C_0 + C_1 + C_2}{C_0C_1C_2}\right)} \tag{19}$$

In this case, only the lower frequency has to be considered because it refers to the first system harmonic, which is consistent with the observed free pressure oscillations.

The period of these fluctuations is given by

$$T = \frac{2\pi}{\omega} \tag{20}$$

The physical and geometrical features of the CR system under investigation determine the following model parameters:

$$C_0 = 6.92 \times 10^{-12}\ \text{m s}^2$$

$$C_1 = 4.46 \times 10^{-13}\ \text{m s}^2$$

$$C_2 = 1.29 \times 10^{-13}\ \text{m s}^2$$

$$L_{01} = 27{,}631\ \text{m}^{-1}$$

$$L_{12} = 31{,}812\ \text{m}^{-1}$$

$$T = 0.8\ \text{ms}$$

The theoretical period of 0.8 ms thus obtained has to be compared with the experimentally evaluated period of nearly 0.85 ms (Fig. 10), which is a fairly good agreement, taking the simplicity of the proposed model into account. Therefore, this model can be used as a predictive tool for evaluating the system oscillation frequency if any geometrical quantity is modified. This is useful in order to know, for each given layout, which ET give rise to hydraulic resonance conditions in the nozzle. Hydraulic resonance occurs when the needle closes as soon as the compression wave, due to the rail reflection of the injection-induced depression wave, reaches the nozzle. Thus, the water hammer due to injector closure and the compression wave coming from the rail are in phase, so as to produce very large oscillations in the nozzle. The time required to a pressure wave to travel from the nozzle to the rail and back is equal to half the free oscillation period T for the considered layout. Therefore, for an assigned system configuration, the solenoid ET, which cause resonance, are around the value $T/2$. For each hydraulic circuit configuration, the ET which produce resonance in the nozzle should be better avoided: For the pilot shot, when pilot and main injections occur and for the main shot, when main and postpulses are involved.

Dynamic Interactions Between Injectors. The proposed model allows one to schematize the system consisting of rail, inlet pipe, and injector as a dynamic system with a main frequency that can be estimated by Eq. (19). Such a system can be subjected to resonating conditions if it is excited by other systems with its same frequency.

Figure 22 plots the pressure at the inlet of Injector 1 and in the rail for single (Fig. 22(*a*)) and multiple (Fig. 22(*b*)) injection events in a complete crankshaft cycle. The operation parameters are $p_{\text{rail}}=1000$ bars and $n=2000$ rpm in both cases; for the single injection ET=1000 μs; for the pilot and main injections ET_{pil} =400 μs and $\text{ET}_{\text{main}}=900$ μs, DT=2300 μs. In this latter case, a sensible interaction between injectors can be observed.

Both figures show how the inlet pressure for Injector 1 oscillates very sensibly, as seen before, when it is the same Injector 1 to operate (first injection cycle on the left side in Fig. 22). But also, when other injectors are operating, the pressure at the inlet of Injector 1 undergoes significant fluctuations. This is explained by the fact that each injector gives rise to a dynamic excitation on the rail with a frequency ω, which in turn excites other injectors with the same frequency. If all the inlet-pipe injector subsystems share the same geometrical features, their frequency is the same and therefore the interactions between different injectors are of particular importance.

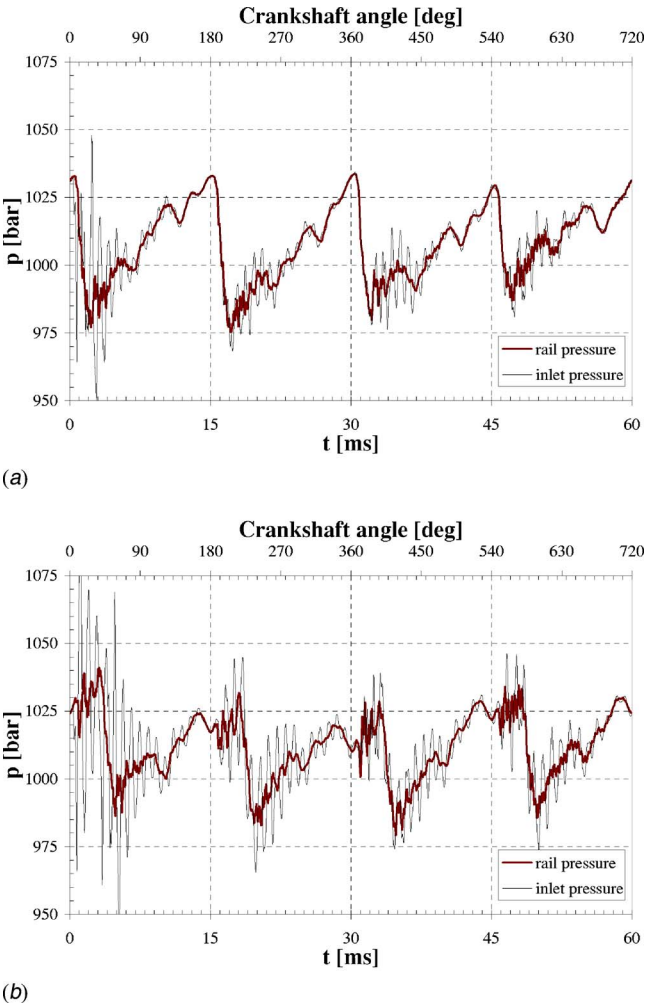

Fig. 22 Pressure distributions at Injector 1 inlet and in the rail: (*a*) main injection only and (*b*) pilot and main injections

Figure 22(*a*) shows that the interaction of other injectors with Injector 1 should not cause disturbances when single injections occur, at least for the present system hydraulic layout, because when Injector 1 is working, the excited pressure fluctuations caused by other injectors are completely damped at injection start. On the other hand, it is evident in Fig. 22(*b*) that adding a pilot injection extends the oscillation duration, which can also be influenced by geometrical modifications, and therefore it is possible to predict that, for some system configurations, injected volume fluctuations could be present also for pilot injections, due to pressure oscillations induced by previous injectors.

Effects of Rail Pressure and Engine Speed on Multiple Injections. The proposed zero-dimensional model gives an insight also into the possible effects of working parameters on the system multiple-injection performance.

The first of these parameters to be taken into account is the rail

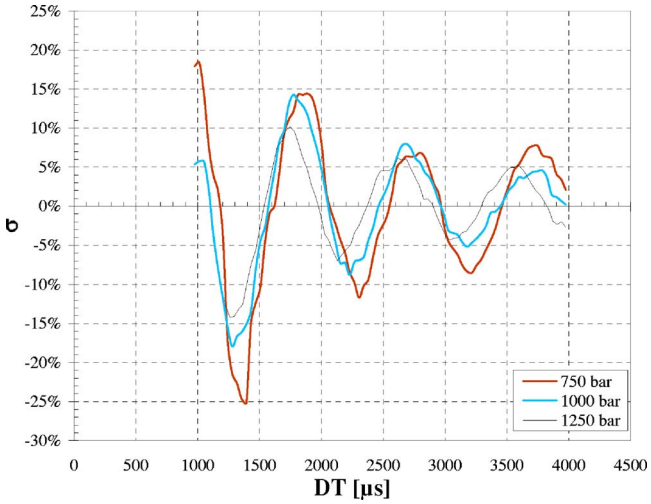

Fig. 23 Main-injection volume deviations for different rail pressures

pressure. The system circular frequencies, from Eq. (19), are slightly modified by pressure values, because these affect the speed of sound a, which is present in hydraulic capacitance definition, Eq. (8). On the other hand, the hydraulic inductance is independent of the pressure level, but depends only on the system geometrical features.

Figure 23 shows the injected volume variations on the main of a double injection, as a function of DT between the pilot and the main injection, for different rail-pressure levels. In this case, operation parameters are $n=2000$ rpm, $ET_{pil}=400$ μs, and $ET_{main}=600$ μs. The main injected volume variations are reported as deviation from its mean value:

$$\sigma = \frac{V_{main} - \bar{V}_{main}}{V_{main}} \times 100 \tag{21}$$

where V_{main} is the main injected volume for each DT and $\bar{V}_{main}$ is its mean value.

It is evident from Fig. 23 that the period T of fluctuations is slightly influenced by the rail pressure, and, in particular, T is smaller for higher pressures. This is consistent with the fact that higher pressures imply higher wave propagation speed.

Figure 24 plots the main injected volume deviation σ versus DT, for pilot and main injections with the same ET as in Fig. 23 and $p_{rail}=1000$ bars, at different engine speeds. It is evident from the figure that the oscillations of the main injected volume are practically independent of the engine speed, because their origin resides in time-dependent phenomena occurring in the system, i.e., wave propagation, and therefore the engine speed is not an influencing factor to be taken into account. However, the same period T turns into different crank-angle intervals if the engine speed varies. Consequently, the main injected volume fluctuations have different periods in the crankshaft-angle domain, whereas they have the same period in the time domain.

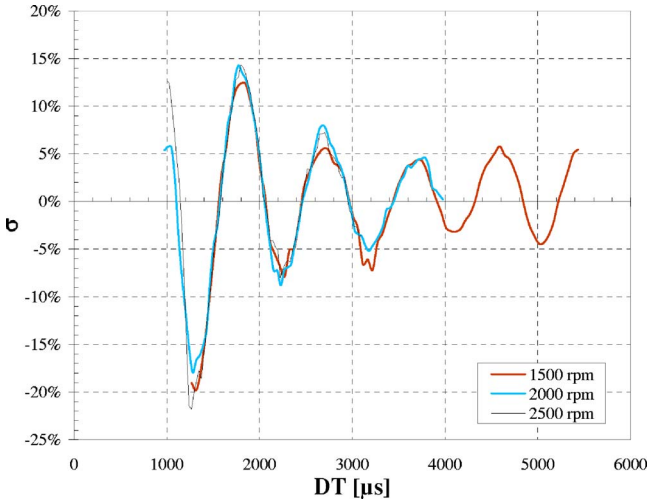

Fig. 24 Main-injection volume deviations for different engine speeds

Dynamics of Mechanical Mobile Elements. The geometrical features of the hydraulic circuit and the dynamic parameters of the injector mobile elements should be selected so as to avoid also mechanical resonance, that is, high oscillations of both control plunger (9 in Fig. 4) and ball valve (5 in Fig. 4), induced by pressure waves in the injection system. Since the damping effect is low in these mechanical systems (the damping factors are less than 0.3, i.e., subcritical), a pressure forcing term with a frequency close to the mobile-element natural frequencies can produce dynamical instabilities in their movement. Thus, it is important in system design to assure that the hydraulic-system natural frequencies are higher than those of the mechanical elements, as far as possible. Calculations with the homemade numerical model developed in Ref. [9] showed that the control plunger stays integral with the needle during both its raising and lowering. This is due to the fact that the control plunger is assembled inside a chamber containing fuel at tank pressure, so that both the needle and the control piston are forced to each other by the pressure actions working on the control-plunger top in the needle-valve control chamber and on the needle side in the delivery chamber. Therefore, the fundamental natural-frequency value of the needle/control-plunger subsystem can be roughly estimated by the following expression for a one-degree of freedom mass-spring system:

$$\lambda = \frac{1}{2\pi}\sqrt{\frac{k_n}{m_n + m_{cp}}} = 250 \text{ Hz} \tag{22}$$

where m_n and m_{cp} are the masses of needle and control plunger, respectively, and k_n is the stiffness of the spring acting on the needle. As was verified, the mechanical natural frequency λ was lower than the hydraulic-circuit frequency, i.e., $1/T \approx 1175$ Hz and therefore no mechanical resonance phenomena occurred. In particular, the pressure-wave fluctuations turned into reduced fluctuation amplitude of the needle-lift temporal pattern.

The pilot valve is made up of two mobile elements, namely, the pin and the armature (or anchor). When the current excites the solenoid, the armature is attracted by the magnet drawing the pin, which is integral with it during the lifting. However, as soon as the pin element reaches the seat, the armature is allowed to travel with respect to the pin valve, so as to damp the counterblow of this element on the basement.

During virtually all the solenoid excitation time, the pin element is stationary at its maximum lift, that is, 40 μm, for the considered electroinjector setting. Therefore, only the armature can undergo mechanical resonance conditions, due to pressure waves, during its free oscillations with respect to the pin valve. The natural frequency of the armature is provided by

$$\lambda = \frac{1}{2\pi}\sqrt{\frac{k_a}{m_a}} = 310 \text{ Hz} \tag{23}$$

m_a being the mass of the armature and k_a the stiffness of the spring acting on the armature. Such a frequency results to be less than the hydraulic natural frequency. A better solution to further reduce the armature oscillations due to pressure waves, without significantly changing the system performance, could be attained by selecting values of the anchor spring stiffness and mass so as to further reduce the natural frequency in Eq. (23).

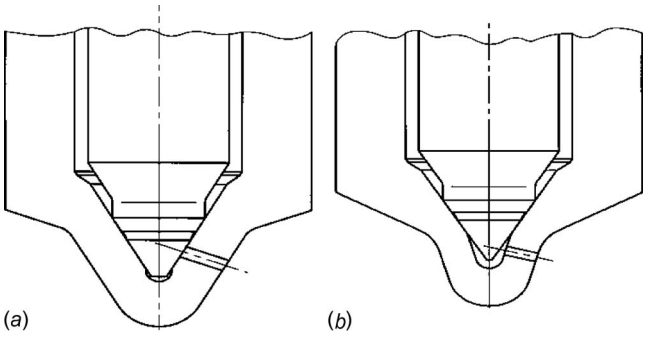

Fig. 25 (*a*) VCO- and (*b*) Minisac-nozzle geometries

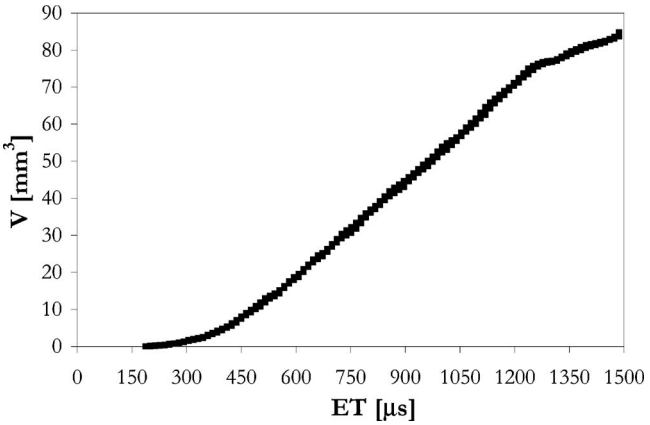

Fig. 27 Cycle-to-cycle variations: Minisac nozzle, p_{rail} = 1000 bars, and n = 2000 rpm

Nozzle Effects on System Dynamics. The nozzle geometry influence on CR injection system dynamic response was evaluated through a comparison between two different nozzles, namely, VCO (Fig. 25(*a*)) and Minisac (Fig. 25(*b*)); the two nozzles share the same number of holes, the same hole diameter, and the same maximum needle lift.

Figure 26 shows the effects of nozzle configuration on the injected flow rate (a) and the injector inlet pressure (b). The injection parameters are p_{rail} = 1000 bars and ET = 1500 μs.

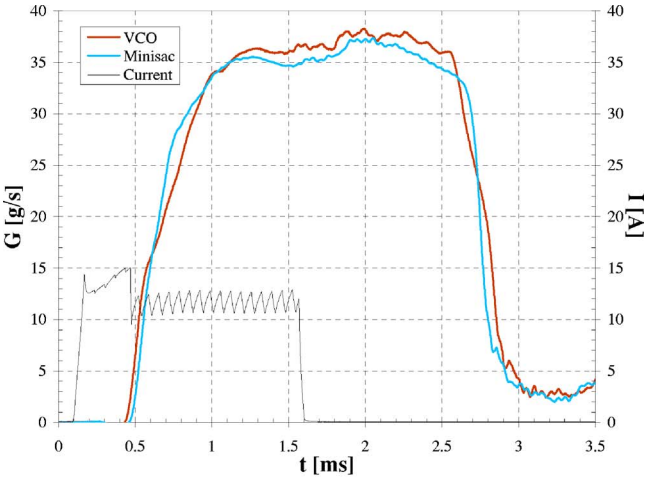

(*a*)

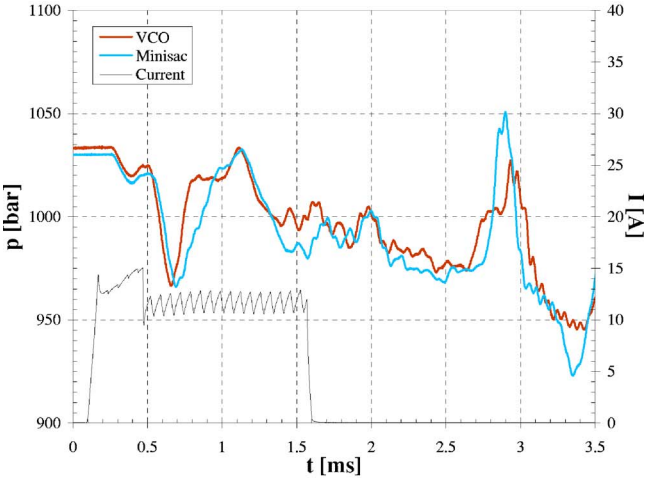

(*b*)

Fig. 26 VCO versus Minisac nozzle: (*a*) injected flow rate and (*b*) inlet pressure

The Minisac nozzle determines a regular flow rate in both the opening and closing phases, whereas the VCO injected flow rate presents a rather uneven pattern in these phases, due to the interference between nozzle tip and injector holes.

Perhaps, more surprising is the sensible influence of nozzle geometry on internal system dynamics. Figure 26(*b*) shows the differences in inlet pressure distributions between VCO and Minisac nozzles. Nevertheless, it should be kept in mind that the nozzle determines the fuel-injection-system boundary condition, so that different behaviors not only in the injected flow rates but also in other system variables are to be expected. In particular, the pressure rise marked as 3 in Fig. 10(*a*) was explained as the result of a compression wave originating from the nozzle. Figure 26(*b*) further substantiates such an explanation, by taking the different time patterns of the pressure rise into account, there. On the other hand, the subsequent pressure rise, marked as 4 in Fig. 10(*a*), does not depend on the nozzle geometry. In fact, as already mentioned, its origin has to be found in the expansion wave due to flow start (marked as 2) and its reflection at the rail.

Another influence of nozzle geometry can be inferred from the pressure peak due to the nozzle closure (Peak 5 in Fig. 10(*b*)). The Minisac nozzle produces a neat and fast closure (as is also shown in Fig. 26(*a*)), and, as a consequence, its pressure peak is rather high with respect to that of VCO geometry. The pressure oscillations arising from the nozzle closing are therefore higher in the case of Minisac-nozzle geometry, and thus in this case, the injected volume fluctuations for multiple injections can be expected to be more pronounced.

Random Cycle-To-Cycle Variations. Experimental tests were made for assessing cycle-to-cycle variations in the injection-system performance. These are due to stochastic dispersions in the whole system mechanics and fluid dynamics that are difficult to separately assess. For a Minisac-nozzle injector, Fig. 27 reports repeated measurement sets of a single injection characteristic. The random fluctuations of V kept less than ± 1.0 mm^3, i.e., relatively low also in consideration of the measurement accuracy (± 0.6 mm^3). A higher dispersion in the injected fuel volume occurred at low nominal rail pressure and engine speed, as shown in Fig. 28. Nevertheless, the cycle-to-cycle variations in this figure are lower than ± 1.3 mm^3.

Figure 29 plots repeated measurement sets of the main fuel volume fluctuations in a pilot-main injection profile (ET_{pil} of 400 μs, ET_{main} of 600 μs, and nominal rail pressure of 1000 bars) when the SOI of the pilot varies. The cycle-to-cycle variation of V with respect to the mean line interpolating the distribution in the figure appears to be low, i.e., comparable to the precision of EMI. This supports the fact that the oscillating behavior of V versus

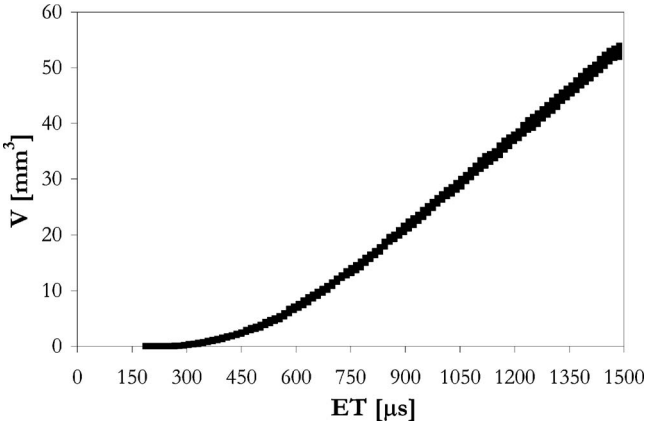

Fig. 28 Cycle-to-cycle variations: Minisac nozzle, p_{rail} = 500 bars, and n = 1500 rpm

SOI_{pilot} is not of stochastic nature but has a deterministic explanation, based on the system pressure-wave dynamics, as illustrated above. For the same system, but with a VCO nozzle, Fig. 30 plots the injection characteristics taken at p_{rail} = 500 bars and n = 1500 rpm in 50 measurement sets. This number of tests was the same as in Figs. 27–29, and was shown to be statistically significant. A slightly higher dispersion was observed at the largest ET values, namely, ± 1.8 mm^3, in comparison to Fig. 28.

With reference to the dispersion in performance of injector production, manufacturer tolerances guarantee that discrepancies in fueling between different injectors do not exceed the bounds reported in Table 1, which refer to Multijet electroinjectors of the latest solenoid generation. In general, the production dispersion of VCO-nozzle injectors is higher than that of Minisac-nozzle injectors. In fact, in VCO nozzles, it is the needle to discover the holes during the initial stage of its lift. Therefore, in these injector types, the position of the needle at rest has a significant influence on the injection flow-rate pattern through the overall hole uncovering stage and, in general, during the nozzle opening and closure phases. Since the needle position at rest undergoes stochastic variations from nozzle to nozzle due to production tolerances, significant performance dispersion can occur among distinct VCO-nozzle injectors.

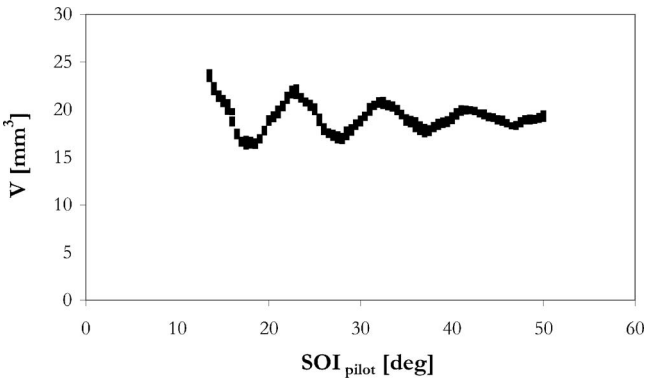

Fig. 29 Cycle-to-cycle variations: Minisac nozzle, p_{rail} = 1000 bars, ET = 400/600 μs, and n = 1500 rpm

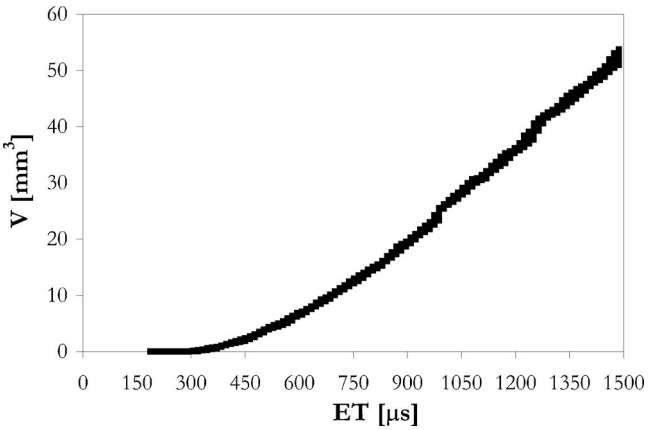

Fig. 30 Cycle-to-cycle variations: VCO nozzle, p_{rail} = 500 bars, and n = 1500 rpm

Table 1 Injector production tolerances

p_{rail} (bar)	ET (μS)	Acceptable dispersion (mm^3)
1400	840	±4.0
800	640	±2.4
800	250	±1.2
300	710	±2.4

Conclusion

An in-depth experimental investigation of CR injection-system dynamics has been performed, with particular emphasis on multiple-injection events.

The highly unsteady wave propagation phenomena taking place in the system play a major role in a proper understanding of important injection-system characteristics, such as injected volume metering and control. In fact, injection-induced pressure oscillations cause a deterministic dependence of injected volume on DT between consecutive injection shots.

In order to obtain a deeper insight into the cause and effect relationship between the injection-triggered pressure-oscillation frequency and the system hydraulic layout, an effective simple zero-dimensional mathematical model was proposed, allowing the characterization of the rail-pipe-injector subsystem natural frequency. This model was shown to be a reliable tool to better understand the CR dynamic behavior, providing a physical interpretation of injected volume oscillations, their dependence on the operating conditions, in addition to possible dynamic interactions between different injectors. It could also give an insight into the influence of geometrical features, such as pipe diameter to length ratio, on system performance. Experimental-theoretical analysis of system layout effects on multiple-injection performance is currently in progress for their optimization.

An analytical relation between the system free oscillation period under a specified layout and the ET that determines hydraulic resonance in the nozzle was provided. Such ET value should be avoided for the pilot shot when pilot and main injections are performed for reducing disturbances on the injected volumes. Furthermore, the hydraulic frequency was compared to the natural frequencies of the mobile elements in order to identify possible mechanical resonance conditions. For the system under investigation, the natural frequency of mobile elements was shown to be lower than the hydraulic circuit one at all considered working conditions and thus the pressure-wave excited fluctuations gave rise to minor oscillation amplitude of valve lift temporal distributions.

From the analysis of system behavior with different nozzle geometries, such as VCO and Minisac, a clear influence of the nozzle configuration reflects not only on the injection flow rate but also on the whole injector fluid-dynamic response and thus on multiple-injection performance.

Finally, experimental tests were carried out to assess cycle-to-cycle variations in the injection-system performance. The stochastic cyclic dispersion is generally small and increases by lowering rail pressure and engine speed.

Acknowledgment

Financial support to this research was provided by Ministry of University and Research (MUR) under COFIN'04 Project, by Fiat Research Center, and by FA-GM Powertrain. The authors would like to thank S. Canale, G. Bonetto, F. Guglielmo, and E. Rigon of Fiat Research Center for their invaluable technical assistance.

Nomenclature

a = speed of sound
A = pipe cross section
C = hydraulic capacitance
d = pipe diameter
DT = dwell time
ET = energizing time
G = injected mass flow rate
I = current
l = pipe length
L = hydraulic inductance
n = engine speed
p = pressure; rail nominal pressure
Q = injected volume flow rate
SOI = start of injection
t = time
T = free oscillation period
u = velocity
V = injected volume; volume
ρ = density
ω = circular frequency; engine speed

Subscripts

a; cp; n = armature; control plunger; needle
main = main injection
pil = pilot injection
rail = rail nominal pressure

References

[1] Stumpp, G., and Ricco, M., 1996, "Common Rail-An Attractive Fuel Injection System for Passenger Car DI Diesel Engines," SAE Paper No. 960870.
[2] Boehner, W., and Hummel, K., 1997, "Common Rail Injection System of Commercial Diesel Vehicles," SAE Paper No. 970345.
[3] Catania, A. E., Ferrari, A., Manno, M., Pellettieri, R., and Spessa, E., 2004, "Development, Setup and Equipment of a High Performance Diesel Injection-System Test Bench: Preliminary Experimental Results on the Dynamics of a CR System," *Proceedings of LIX ATI Congress*, Vol. 2, pp. 821–834, in Italian.
[4] Catalano, L. A., Tondolo, V. A., and Dadone, A., 2002, "Dynamic Rise of Pressure in the Common-Rail Fuel Injection System," SAE Paper No. 2002-01-0210.
[5] Henein, N. A., Lai, M.-C., Singh, I. P., Zhong, L., and Han, J., 2002, "Characteristics of a Common Rail Diesel Injection System Under Pilot and Post Injection Modes," SAE Paper No. 2002-01-0218.
[6] Bianchi, G. M., Falfari, S., Pelloni, P., Filicori, F., and Milani, M., 2002, "A Numerical and Experimental Study Towards Possible Improvements of Common Rail Injectors," SAE Paper No. 2002-01-0500.
[7] Mulemane, A., Han, J.-S., Lu, P.-H., Yonn, S.-J., and Lai, M.-C., 2004, "Modeling Dynamic Behavior of Diesel Fuel Injection Systems," SAE Paper No. 2004-01-0536.
[8] Torkzadeh, D. D., Kiencke, U., and Keppler, M., 2002, "Introduction of a New Non-Invasive Pressure Sensor for Common-Rail Systems," SAE Paper No. 2002-01-0842.
[9] Catania, A. E., Ferrari, A., and Manno, M., 2005, "Development and Application of a Complete Common-Rail Injection System Mathematical Model for Hydrodynamics Analysis and Diagnostics," ASME ICE Spring Technical Conference, Chicago, IL, Apr. 5–7, Paper No. ICES 2005-1018; Trans. ASME: J. Eng. Gas Turbines Power, in press.
[10] Bosch, W., 1966, "The Fuel Rate Indicator: A New Measuring Instrument for Display of the Characteristics of Individual Injection," SAE Paper No. 660749.
[11] R. Bosch, GmbH, 1999, *Diesel-Engine Management*, Bosch Technical Books, SAE International, Detroit.
[12] LeVeque, R. J., 1992, *Numerical Methods for Conservation Laws*, Birkhäuser, Basel.
[13] Catania, A. E., Ferrari, A., and Spessa, E., 2006, "Numerical-Experimental Study and Solutions to Reduce the Dwell Time Threshold for Fusion-Free Consecutive Injections in a Multijet Solenoid-Type CR Systems," ASME Paper No. ICES2006-1369, ASME Technical Paper Award for Best ICES2006 Paper; Trans. ASME: J. Eng. Gas Turbines Power, in press.